



Contents lists available at SciVerse ScienceDirect

BioSystems

journal homepage: [www.elsevier.com/locate/biosystems](http://www.elsevier.com/locate/biosystems)

# Insight into the binding mode and the structural features of the pyrimidine derivatives as human A<sub>2A</sub> adenosine receptor antagonists

Lihui Zhang<sup>a</sup>, Tianjun Liu<sup>b,\*\*</sup>, Xia Wang<sup>a</sup>, Jinan Wang<sup>a</sup>, Guohui Li<sup>c</sup>, Yan Li<sup>d</sup>, Ling Yang<sup>e</sup>, Yonghua Wang<sup>a,\*</sup>

<sup>a</sup> Bioinformatics Center, Northwest A & F University, Yangling, Shaanxi 712100, China

<sup>b</sup> College of Economics and Management, Northwest A & F University, Yangling, Shaanxi 712100, China

<sup>c</sup> Laboratory of Molecular Modeling and Design, Chinese Academy of Sciences, Dalian, Liaoning 116024, China

<sup>d</sup> School of Chemical Engineering, Dalian University of Technology, Dalian, Liaoning 116012, China

<sup>e</sup> Laboratory of Pharmaceutical Resource Discovery, Dalian Institute of Chemical Physics, The Chinese Academy of Sciences, Dalian, Liaoning 116023, China

## ARTICLE INFO

### Article history:

Received 23 January 2013

Received in revised form 7 April 2013

Accepted 24 April 2013

### Keywords:

Pyrimidine derivatives

Human A<sub>2A</sub> adenosine receptor

Molecular docking

Molecular dynamics

Thermodynamic analysis

3D-QSAR

## ABSTRACT

The interaction of 278 monocyclic and bicyclic pyrimidine derivatives with human A<sub>2A</sub> adenosine receptor (AR) was investigated by employing molecular dynamics, thermodynamic analysis and three-dimensional quantitative structure–activity relationship (3D-QSAR) approaches. The binding analysis reveals that the pyrimidine derivatives are anchored in TM2, 3, 5, 6 and 7 of A<sub>2A</sub> AR by the aromatic stacking and hydrogen bonding interactions. The key residues involving Phe168, Glu169, and Asn253 stabilize the monocyclic and bicyclic cores of inhibitors. The thermodynamic analysis by molecular mechanics/Poisson Boltzmann surface area (MM-PBSA) approach also confirms the reasonableness of the binding modes. In addition, the ligand-/receptor-based comparative molecular similarity indices analysis (CoMSIA) models of high statistical significance were generated and the resulting contour maps correlate well with the structural features of the antagonists essential for high A<sub>2A</sub> AR affinity. A minor/bulky group with negative charge at C2/C6 of pyrimidine ring respectively enhances the activity for all these pyrimidine derivatives. Particularly, the higher electron density of the ring in the bicyclic derivatives, the more potent the antagonists. The obtained results might be helpful in rational design of novel candidate of A<sub>2A</sub> adenosine receptor antagonist for treatment of Parkinson's disease.

© 2013 Elsevier Ireland Ltd. All rights reserved.

## 1. Introduction

Human adenosine receptors are members of seven transmembrane-spanning G protein-coupled receptor (GPCR) superfamily, delineated into four subtypes namely the A<sub>1</sub>, A<sub>2A</sub>, A<sub>2B</sub> and A<sub>3</sub> receptors, which have been considered as potential therapies for neurodegenerative (Morelli et al., 2009), immune, and inflammatory disorders (Blackburn et al., 2009), cancer (Fishman et al., 2009) and cardiac disease (Headrick and Lasley, 2009). Among them, the A<sub>2A</sub> adenosine receptor (A<sub>2A</sub> AR) is highly expressed in the basal ganglia and functionally coupled with the activity of dopamine-sensitive neurons (Drabczynska et al., 2011). Recent evidences (Bara-Jimenez et al., 2003; Jenner et al., 2009; Ongini et al., 1997; Richardson et al., 1997) have highlighted A<sub>2A</sub> AR as a potential therapeutic target for diseases such as Parkinson's disease (PD), which is a neurodegenerative disorder characterized

by motor dysfunctions arising from the underlying degeneration of dopaminergic neurons of the basal ganglia (Frau et al., 2011; Schwarzschild et al., 2006). Antagonism of the A<sub>2A</sub> AR reduces adenosine signaling, enhances the sensitivity of the dopaminergic neurons and restores balance to the signaling pathway controlling over muscle movement (Fenu et al., 1997; Kanda et al., 1998), thus results in lessening effectively motor dysfunctions of PD.

For the binding of the A<sub>2A</sub> AR antagonists, the amino acids in transmembrane helix (TMs) 3, 5, 6, and 7 of A<sub>2A</sub> AR are vital, which are indicated by the previously site-directed mutagenesis assays (Carlsson et al., 2010; Ivanov et al., 2007). Mutations of some residues, such as Glu169(TM5), His250(TM6), Asn253(TM6) and Ile274(TM7), disrupt antagonist interactions resulting in the dramatic loss of binding, while the replacements of Ser277(TM7) and Ser281(TM7) produce moderate changes in binding affinities (Cristalli et al., 2008; Kim et al., 1995, 2003). Recently, the structures of the membrane-spanning heptahelical domain of human A<sub>2A</sub> AR with antagonists have been solved employing X-ray crystallography (Congreve et al., 2012; Dore et al., 2011; Jaakola et al., 2008). The key residues obtained from the mutagenesis studies directly contact with the bound antagonists by hydrogen bonding and hydrophobic interaction (Dore et al., 2011). Besides, a  $\pi$ -stacking

\* Corresponding author. Tel.: +86 029 87092262.

\*\* Corresponding author. Tel.: +86 029 87081157.

E-mail addresses: Ltj168168@126.com (T. Liu), yh\_wang@nwsuaf.edu.cn (Y. Wang).

interaction between Phe168(TM5) and the heterocyclic moiety of the ligands provides additional driving force for stable binding of the A<sub>2A</sub> antagonists (Ivanov et al., 2009; Kiran et al., 2012). However, among these key sites, it remains ambiguous whether all antagonists with diverse structures interact at the same site, or multiple sites within the A<sub>2A</sub> receptor.

The early developed adenosine receptor antagonists are xanthines, such as caffeine and theophylline, which display poor pharmacophysiological properties and no selectivity for A<sub>2A</sub> receptor (Sauer et al., 2000). After modification of the xanthine nucleus, the selective 8-styrylxanthine derivatives were developed. However, low water solubility has hindered further application of these compounds (Kase et al., 2003). Thus considerable interests have been concentrated in development of well tolerated and orally bioavailable antagonists, stradefylline for example (Knutsen and Weiss, 2001), which has completed the clinical trials for treating Parkinson's disease (Bara-Jimenez et al., 2003). Unfortunately, it failed to meet the primary end-point of efficacy trials and was declined by FDA in 2008 (Gillespie et al., 2009a). To quest more A<sub>2A</sub> antagonists with higher potency, the non-xanthine type heterocyclic antagonists have been developed, which exhibited excellent preclinical physiochemical and pharmacokinetic profiles (Gillespie et al., 2008a, 2008b, 2008c, 2009a, 2009b, 2009c), and some of which have displayed strong in vivo potency and high oral bio-availability. Particularly, the compound 3-(3-methyl-4-amino-benzyl)-5-amino-7-(furan-2-yl)-triazolo[4,5-d]-pyrimidine has successfully completed phase I clinical study (Gillespie et al., 2009a). However, the discovery of high selective, potent and well tolerated antagonists with good oral bioavailability still remains to be a big challenge. In order to facilitate the drug discovery process, in silico methods as a productive and cost-effective technology, such molecular modeling, three-dimensional quantitative structure–activity relationship (3D-QSAR) analysis, can be used in combination with experimental practices.

Recently, 3D-QSAR analysis has been employed to probe the structural features of the A<sub>2A</sub> antagonists, such as pyrazolo-triazolo-pyrimidine antagonists (Michielan et al., 2008). The specific structural features defined by the comparative molecular field analysis (CoMFA) and comparative molecular similarity indices analysis (CoMSIA) are essential for enhancing ligand-binding affinity in the A<sub>2A</sub> AR. A negative charge on the heterocyclic nitrogen, together with volume and lipophilicity of the whole molecules are important contributors to the selectivity of adenosine antagonists. However, there still exist several problems about the molecular mechanism of pyrimidine derivatives as antagonists of human A<sub>2A</sub> AR: (1) How do the derivatives interact with the human A<sub>2A</sub> AR? (2) What is the similarity/difference of the binding sites between these antagonists and other known A<sub>2A</sub> antagonists? (3) What are the structural features of the derivatives indispensable for improvement of the potency? Here, the combination of molecular docking, molecular dynamics and thermodynamic analysis is performed to elucidate the probable binding mode of the antagonists within the human A<sub>2A</sub> AR. In addition, 3D-QSAR analyses using the CoMFA and CoMSIA methodologies are employed to insight into the structural features of these derivatives. The mechanism of interaction of the pyrimidine derivatives with the A<sub>2A</sub> AR and the characteristic structure of the derivatives might facilitate discovery of more efficient drug candidates for the treatment of PD.

## 2. Materials and methods

### 2.1. Data set

278 monocyclic and bicyclic pyrimidine derivatives (Gillespie et al., 2008a, 2008b, 2008c, 2009b, 2009c, 2009d) as the

human A<sub>2A</sub> AR antagonist were collected with a wide activity ranging from 5.2 to 9.2 (pK<sub>i</sub> values, converted by the corresponding K<sub>i</sub> values), which were classified artificially into three classes, i.e., **I**: pyrimidine and triazine derivatives (97 compounds); **II**: pyrazolo[3,4-d]pyrimidines, pyrrolo[2,3-d]pyrimidines, triazolo[4,5-d]pyrimidines and 6-arylpurines (120 compounds); **III**: thieno[3,2-d]pyrimidines (61 compounds). All compounds of each class were used as a dataset and then divided into a training set and a test set in a ratio of 3:1 by considering both the distribution of the inhibitory activity and the structural diversity. The training set was used to construct 3D-QSAR models and the test set (asterisked molecules in Table S1) was kept to test the actual prediction of the model. All molecules of three datasets with structures and biological data (pK<sub>i</sub>) are shown in Table S1 (Supplementary data).

### 2.2. Molecular modeling and alignment

The three-dimensional models of all compounds were constructed by using the SYBYL package (Tripos Associates, St. Louis, MO, USA). All compounds were added with Gasteiger–Huckel charges and minimized using the Tripos force field (Clark et al., 1989) with the distance-dependent dielectric and the Powell gradient algorithm (convergence criterion of 0.05 kcal/mol). Two different alignment methods, namely, the ligand- and receptor-based alignments, were adopted to obtain the optimal 3D-QSAR model. In the first method, all compounds in each dataset were aligned to the template compound (**I** 92, **II** 111, and **III** 45 selected based on the highest potency) by the Align-Database function in SYBYL package. In the second method, the bioactive conformations of all compounds were firstly derived from docking and then processed by means of the first method. The details have been described in our previous work (Wang et al., 2010; Zhang et al., 2011).

### 2.3. Docking

In order to compare the binding sites, the latest A<sub>2A</sub> AR (3PWH.pdb) with some mutations in the crystal structure (3EMS.pdb) was chosen, obtained from the Protein Data Bank (<http://www.rcsb.org/pdb>). The missing residues from 150 to 157 in the EL2 region were reconstructed by using MODELLER software (Sali and Blundell, 1993). The missing hydrogen atoms and side-chain were added in stereochemically preferred conformations. Then, Kollman charges were added to the protein, while Gasteiger–Hückel charges (Gasteiger and Marsili, 1980) were assigned to all ligands. Subsequently, docking was performed with Autodock using Lamarckian Genetic Algorithm (LGA) (Morris et al., 1998). For each kind of ligand atoms, 60 Å × 60 Å × 60 Å 3D grids centered on the binding site with 0.375 Å spacing were calculated using Auto-grid3 (Morris et al., 1996). Parameters for the docking are as follows: random starting position and conformation; population size of 50; maximal mutation of 2 Å in translation and 50 degrees in rotations; maximal energy evaluations of 2.5 × 10<sup>6</sup> and maximal generations of 2.7 × 10<sup>4</sup>; elitism of 1; mutation rate of 0.02 and crossover rate of 0.8; local search frequency of 0.06; and 1.5 million energy evaluations (Osterberg et al., 2002). After 100 trials of each docking, the more energetically favorable conformations of all compounds were selected by comparing docking poses and considering the total energy value, and then aligned together for CoMFA and CoMSIA modeling. The docked complexes with the most potent compound in each class were selected for subsequent analyses.

## 2.4. Molecular dynamics simulation

MD simulations for these docked complexes were implemented with the Gromacs 4.5.4 (Hess et al., 2008) package. Each complex was soaked in a SPC water box (Berendsen and Strutsma, 1987), keeping a minimum distance of 10 Å between the solute and each face of the box. The system was neutralized by adding 7 Cl<sup>-</sup> counterions. The Gaff (Wang et al., 2004) and AMBER99 (Hummer et al., 2001) force fields were used to describe the ligand and protein, respectively. To release the internal strain energies of the entire system gradually, the whole system was subjected to 50,000 steps of energy minimization. Subsequently, MD simulation of 200 ps at 300 K and 1 atm was performed to equilibrate the system and to adjust the density of the solvation box. After all these preparative steps, a production simulation of 10 ns long was performed with the time interval of 2 fs under constant temperature (300 K) and pressure (1 atm). Temperature of the system was controlled by a V-rescale thermostat (Bussi et al., 2007) with the coupling constant of 0.1 ps, and pressure were regulated by the Parrinello–Rahman pressure coupling method (Parrinello, 1981). The particle-mesh-Ewald (PME) method (Darden et al., 1993) was employed to treat the long-range electrostatic interaction with a cut off of 10.0 Å. During the entire simulation process, the coordinate trajectory of each system was recorded every 2 ps for subsequent analyses.

## 2.5. Binding free energy calculation

The binding free energies of all the systems obtained from the last 500 snapshots MD trajectories were calculated by using the molecular mechanics/Poisson Boltzmann surface area (MM-PBSA) approach integrated in AMBER 10 (Case et al., 2008). The following expression was used to describe the binding free energy ( $\Delta G_{\text{bind}}$ ):

$$\Delta G_{\text{bind}} = \Delta H_{\text{bind}} - T\Delta S_{\text{bind}} \quad (1)$$

$$\Delta H_{\text{bind}} = \Delta E_{\text{gas}} + \Delta G_{\text{solv}} \quad (2)$$

$$\Delta E_{\text{gas}} = \Delta E_{\text{ele}} + \Delta E_{\text{vdW}} + \Delta E_{\text{int}} \quad (3)$$

$$\Delta G_{\text{solv}} = \Delta G_{\text{PB}} + \Delta G_{\text{nonpolar}} \quad (4)$$

$$\Delta G_{\text{nonpolar}} = \gamma(\text{SASA}) + \beta \quad (5)$$

Molecular mechanical free energy ( $\Delta E_{\text{gas}}$ ) was divided into contributions from the electrostatic potential ( $\Delta E_{\text{ele}}$ ) and the van der Waals ( $\Delta E_{\text{vdW}}$ ) potential. Solvation free energy ( $\Delta G_{\text{solv}}$ ) was composed of two parts, the polar solvation free energy ( $\Delta G_{\text{PB}}$ ) and the nonpolar solvation free energy ( $\Delta G_{\text{nonpolar}}$ ). The nonpolar solvation energy was calculated based on the solvent-accessible surface area (SASA) which was estimated using the Molsurf program with a probe radius of 1.4 Å (Sanner et al., 1966), as well as the parameters of  $\gamma = 0.00542 \text{ kcal}/\text{\AA}^2$  and  $\beta = 0.92 \text{ kcal}/\text{mol}$ . The dielectric constant was set to 1 for the interior solute and 80 for the exterior solvent. The final  $\Delta E_{\text{gas}}$  and  $\Delta G_{\text{solv}}$  values for each protein–ligand binding mode were taken as the averages of the respective  $\Delta E_{\text{gas}}$  and  $\Delta G_{\text{solv}}$  values. To evaluate entropy contributions ( $T\Delta S$ ), a full energy minimization was first performed on each species (receptor, ligand, or complex) prior to the normal-mode analysis.

## 2.6. 3D-QSAR analysis

CoMFA and CoMSIA analyses are performed to construct good predictive QSAR models and to analyze the effect of each field on the activities of the pyrimidine derivatives. In CoMFA, the steric (S) and electrostatic (E) potential fields were calculated by using the Tripos

force field (Clark et al., 1989) at each lattice intersection of a regularly spaced (2 Å) grid. A sp<sup>3</sup> carbon atom with radius 1 Å and charge +1 was served as the probe atom to calculate the fields. The steric and electrostatic contributions were truncated at a default value (30 kcal/mol). In CoMSIA, five similarity indices descriptors—steric (S), electrostatic (E), hydrophobic (H), hydrogen bond donor (D) and hydrogen bond acceptor (A), were calculated at the same lattice box used in the CoMFA calculations with a common probe atom of 1 Å radius, as well as the charge, hydrophobicity, and hydrogen bond properties of +1. CoMSIA similarity indices (AF) for a molecule *j* with atoms *i* at the grid point *q* are calculated by Eq. (1') as follows:

$$A_{F,K}^q(j) = - \sum \omega_{\text{probe},k} \omega_{ik} e^{-\alpha r_{iq}^2} \quad (1')$$

where *k* represents the steric, electrostatic, hydrophobic, hydrogen-bond donor and acceptor properties; *i* is the summation index over all atoms of the molecule *j* under investigation;  $\omega_{ik}$  is the actual value of the physicochemical property *k* of atom *i*;  $r_{iq}$  is the mutual distance between probe atom at grid point *q* and atom *i* of the test molecule;  $\omega_{\text{probe},k}$  is the value of the probe atom. The attenuation factor  $\alpha$  was set to the default value of 0.3.

Partial least-squares (PLS) method was applied to generate 3D-QSAR models by linearly correlating the CoMFA/CoMSIA descriptors to the observed biological activities. To build more reasonable QSAR models, molecular descriptors were calculated using the DRAGON (<http://www.taletе.mi.it/index.htm>), and selected using the stepwise linear regression method in R software ([www.r-project.org](http://www.r-project.org)). The best relevant and meaningful descriptors were further put into the PLS analysis. In this method, the optimal number (*N<sub>c</sub>*) of components was determined by leave-one-out (LOO) cross-validation method with a cross-validation coefficient ( $q^2$ ). Non-cross-validated correlation coefficient ( $r_{\text{ncv}}^2$ ) was calculated subsequently based on the optimum number of components. In addition, the statistical significance of the models was described by the standard error of estimate (SEE) and ratio of  $r_{\text{ncv}}^2$  (*F*) and standard error of prediction (SEP). The predictive correlation coefficient  $r_{\text{pred}}^2$ , based on the test set molecules, was calculated using Eq. (2').

$$r_{\text{pred}}^2 = 1 - \left( \frac{\text{PRESS}}{\text{SD}} \right) \quad (2')$$

where SD is the sum of squared deviations between the biological activities of the test set molecules and the mean activities of the training set molecules, and PRESS is the sum of squared deviation between the actual and predicted activities of the test set molecules. The CoMFA/CoMSIA results were graphically interpreted by field contribution maps using the “STDEV\*COEFF” field type. To validate the 3D-QSAR models, the rm2 metrics for all the three datasets were calculated using this web application (accessible from <http://aptsoftware.co.in/rmsquare/>) (Ojha et al., 2011; Roy et al., 2012, 2013).

## 3. Results and discussion

### 3.1. Binding mode of human A<sub>2A</sub> adenosine receptor

In the present study, dockings of all compounds into the human A<sub>2A</sub> AR were carried out, and the docked complexes of A<sub>2A</sub> AR with the most active ligands (I 92, II 111, and III 45) were chosen as the templates to study the binding modes of the ligands in the receptor. To obtain the “real” bioactive conformation, 10 ns molecular dynamic simulation was employed to make the structure of the docking complex more reasonable by considering both the impacts of the receptor flexibility and the effects of water solvation on the complex. After 6 ns, all complexes reached a stable conformation

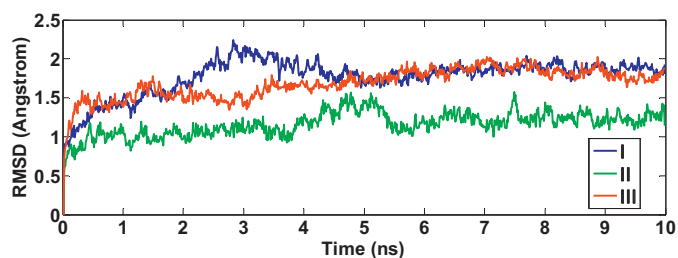


**Fig. 1.** Plot of the root-mean-square deviation (RMSD) of the docked complex structures of human  $A_{2A}$  adenosine receptor with the ligand (I 92, II 111, and III 45) versus the MD simulation time.

revealed by root-mean-square deviation (RMSD, Fig. 1), which were then extracted as the candidate for the subsequent binding study.

As illustrated in Fig. 2, the binding poses for three kinds of the derivatives reveal a similar binding mode within the  $A_{2A}$  AR. This common binding motif involves polar interactions with Glu169(5.30) and Asn253(6.55) side chain, non-polar interactions with Val84(3.32), Leu249(6.51), Met270(7.35) and Ile274(7.39), as well as  $\pi$ -stacking between aromatic moieties of the ligands and the conserved Phe168 (5.29) side chain of the receptor (Residue numbers in parentheses are based on Ballesteros–Weinstein nomenclature 42) (Ballesteros and Weinstein, 1995). Moreover, during all simulations, we find that Asn253(6.55) are capable of forming stable H-bonding with ligands, indicating that this residue plays a key role in maintaining the binding poses of different heterocyclic compounds. Interestingly, mutations of these H-bonding residues (Glu169(5.30), Asn253(6.55), Leu249(6.51), His250(6.52) and His278(7.43) as shown in Fig. 2), have been reported to disrupt antagonist interactions (Jaakola et al., 2010; Langmead et al., 2012). Additionally, the aromatic  $\pi$ -stacking interactions between Phe168(5.29) and the heterocyclic core of the ligands are essential for high affinity of the antagonist, which has been demonstrated by homology modeling and mutation studies (Ivanov et al., 2009; Jaakola et al., 2010).

In addition to these core interactions, the  $A_{2A}$  AR antagonists have an aromatic group extending deeper into the binding pocket

and/or flexible extensions toward the extracellular opening of the pocket. The imidazol-2-yl-methyl-NHCO moiety of Fig. 2A stretches toward TM6 and TM7 helix and deepens into a large pocket, suggesting that this part of the pocket can be exploited in ligand design. This imidazole ring is approximately 3.3 Å away from the so-called “toggle-switch” Trp246(6.48), and we speculate that the hydrophobic interaction between the imidazole ring and Trp246(6.48) will hinder the structural rearrangements necessary for activation, constraining the receptor in an inactive state (Jaakola et al., 2010). In Fig. 2B, the compound's (3-F-4-NH2)-benzyl moiety is also extended downward into the binding pocket and forms a hydrogen bond network with Ala59(2.57), Phe62(2.60), Ala63(2.61) and Ile80(3.28). The 4-methyl-thiazolyl moiety (Fig. 2C) extends toward TM5 and TM6 helix to make more favorable contacts with the binding pocket side chains. In addition, the furan moiety stretches to form predominantly hydrophobic interactions in the large pocket. In summary, we predicted that the  $\pi$ -stacking interaction with Phe168(5.29) and hydrogen bonds with the Glu169(5.30) and Asn253(6.55) side chains are key features for the binding of the pyrimidine derivatives to the TM2, 3, 5, 6 and 7 of  $A_{2A}$  AR.

A comparison of the binding poses of  $A_{2A}$  antagonist is made, contained the above derivatives, ZM241385 ((4-(2-[7-amino-2-(2-furyl)[1,2,4]-triazolo[2,3-a][1,3,5]triazin-5-yl amino]ethyl)phenol)), the xanthines xanthine amine congener (XAC) and caffeine in the crystal structure (Code: 3PWH, 3RFM and 3REY). ZM241385, XAC and caffeine bind in a similar position, mainly anchored by an aromatic stacking interaction with Phe168 from the second extracellular loop (ECL2), an aliphatic hydrophobic interaction with Ile274 and a hydrogen bonding interaction with Asn253 (Dore et al., 2011). These interactions are the same as that in the pyrimidine binding mode, playing a central role in coordinating the ring core of the  $A_{2A}$  antagonists. Besides, the hydrophobic surface supplied by Leu249 and Met270 is a common feature of the binding for these antagonists. Additionally, the non-planar configuration of antagonists accommodated by the pocket may result in different conformational preferences for the  $A_{2A}$  AR, potentially leading to unusual binding and/or functional properties of these ligands, such as the interactions with Ala63, Val84, His250 and His278. However, they differ in that Glu169

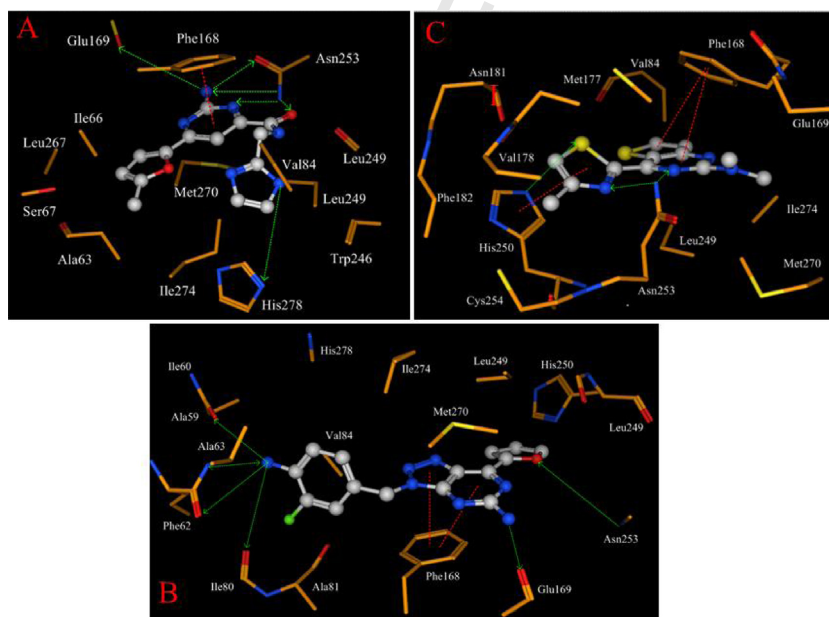


**Fig. 2.** Docked conformation derived for compounds (I 92, II 111, and III 45) with the allosteric binding site of  $A_{2A}$  AR. Model compound and allosteric binding site amino acid residues are shown as stick representation. Hydrogen bonding interactions are shown as green arrowhead lines; the aromatic  $\pi$ -stacking interactions are shown as red dashed lines. The nonpolar hydrogen was removed for clarity. (Red atom: oxygen; blue: nitrogen; yellow atom: sulfur; green atom: fluorine). (For interpretation of the references to color in this figure legend, the reader is referred to the web version of this article.)

**Table 1**  
Binding free energy estimates for the docking complexes of A<sub>2A</sub> AR with the ligands.

	$\Delta E_{\text{ele}}$	$\Delta E_{\text{vdw}}$	$\Delta E_{\text{gas}}$	$\Delta G_{\text{PB}}$	$\Delta G_{\text{nonpolar}}$	$\Delta G_{\text{solv}}$	$T\Delta S_{\text{bind}}$	$\Delta G_{\text{bind}}$
I	-17.2	-43.7	-60.9	21.7	-5.65	16.03	-15.04	-29.78
II	-7.5	-44.2	-51.7	14.4	-5.73	8.67	-10.78	-32.26
III	-0.65	-37.8	-38.5	9.47	-5.29	4.18	-17.63	-16.65

in the pyrimidine mode plays an important H-bond acceptor in the structure–activity relationship, whereas in other modes it has a less prominent role in the binding (Dore et al., 2011). In a word, all candidate chemotypes of A<sub>2A</sub> antagonists are predicted to share key features in the binding mode within the crystal structure, including stacking interaction with Phe168, H-bond interactions with Asn253 and Glu169 side chains, as well as an aliphatic hydrophobic interaction with Ile274. The binding analysis presented above provides us with rich information about the mechanism of interaction of the antagonists with A<sub>2A</sub> AR, and this in turn facilitates our ability to understand and further optimize the interaction components for the pyrimidine derivatives binding to the receptor.

### 3.2. Binding free energies

MM-PBSA calculations were performed to calculate the binding free energies for all of the MD-simulated binding structures, and the calculated free binding energies with the individual energy contributions are summarized in Table 1. We note that the binding free energies are determined by all of the contributions from the protein–ligand interactions in the gas phase, solvation/desolvation effects, and entropy change.

For all binding modes, the gas energies for ligands in A<sub>2A</sub> AR are the dominant contributor to interactive energies, which vary among the three models. By further inspection of the individual gas energy, it is clearly seen that the electrostatic contribution tilts the balance toward a positive overall free energy of binding, with the large variation for three models. The van der Waals interaction energy contributes most to the binding of the ligands for all the models. The solvation energy is a key element in correctly ranking inhibitors belonging to the same family. However, the positive energies are unfavorable for the binding, indicating that all the ligands are badly exposed to water interactions in the complex. The nonpolar solvation energy contributes identically to the ligands, while the polar solvation affects the binding of the ligands in an unfavorable way. Considering the entropy term, the calculated binding free energies indicate that the bindings of the pyrimidine derivatives in A<sub>2A</sub> AR are stable and reasonable, and the rank is in good agreement with that of the experimental ligand activities.

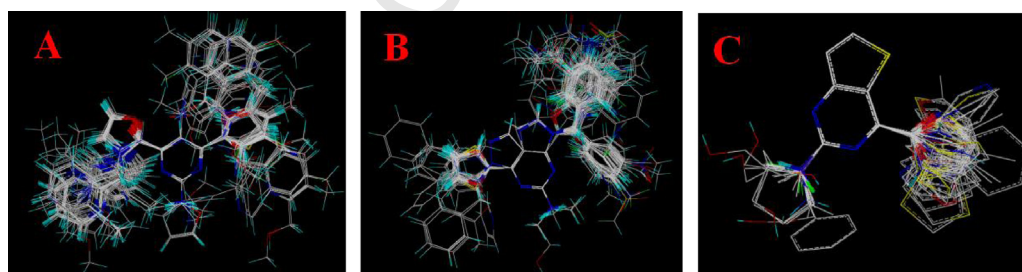
### 3.3. 3D-QSAR models

For the prediction of the binding affinity to human A<sub>2A</sub> AR, 3D-QSAR analysis was applied to the pK<sub>i</sub> of three sets of the pyrimidine

derivatives based on the ligand-/receptor-based guided alignments. The composite structure diagram after alignment (Fig. 3) displays the structures of all compounds superimposed and illustrates how the structurally diverse set of compounds allow for a comprehensive probing of the effects of structural modifications in all regions. In this work, several CoMFA and CoMSIA models were developed. The best models are selected according to the best statistical results of PLS analysis, the greatest predictive power for the external test set and the good consistency between 3D-QSAR maps and docking results. Moreover, the qualities of the final models are assessed by inspection of the dispersion plots of the predicted versus experimental values (Fig. 4).

To build more reasonable QSAR models, several relevant and meaningful molecular descriptors (Table 2) were added into the PLS analysis. The involved descriptors in the model II are constitutional as follow: (i) two 3D-MorSE descriptors: Mor21m, signal 21/weighted by atomic masses; Mor22e, signal 22/weighted by atomic Sanderson electronegativities. 3D-MorSE descriptors take into account the 3D arrangement of the atoms without ambiguities (in contrast with those coming from chemical graphs), and indicate that atomic mass and electronegativity of a compound are concerned with the inhibitory activity. (ii) A molecular property: AlogP, the octanol–water partition Coefficient (log P) that is related to the hydrophobic character of the molecule describing effects such as the solvent behavior, polarizability, and partitioning through a cell wall (Culler et al., 1996). It does well describe the bioavailability of a compound to the organism. In addition, two molecular descriptors of the model III are Mor25m (3D-MorSE signal 25/weighted by atomic masses) and Mats5v (Moran autocorrelation – lag 5/weighted by atomic van der Waals Volumes), seeming that the inhibitory activity of the compounds is modulated with a subtle balance of the two fields.

Table 3 gives a summary of the PLS analysis for the best models selected and reports the relative contributions of each model together with the optimal number of components,  $q^2$ ,  $r_{\text{ncv}}^2$ , SEE,  $F$ , SEP and  $r_{\text{pred}}^2$ . All the statistical parameters are reasonably high, which highlight the stability and predictability of the models. Further, the calculated average  $r_m^2$  and  $\Delta r_m^2$  values (Table 3) suggest the predictability of the models (for an acceptable QSAR model, the value of “Average rm2” should be >0.5 and  $\Delta r_m^2$  should be <0.2) (Ojha et al., 2011; Roy and Mitra, 2012). It is noteworthy to find that the S, E and D fields comprehensively affect the inhibition potency of all pyrimidine derivatives. However, the compounds (I: 23, 27, 35, 54, 59; II: 10, 15, 32, 40, 60, 106; III: 8, 27, 42) regarded as outliers were omitted from the final analysis, since their differences

**Fig. 3.** Superimposition of all compounds in the training and test sets with common substructure shown in the upper left corner. (A) I: ligand-based alignment, (B) II: ligand-based alignment, (C) III: receptor-based alignment.

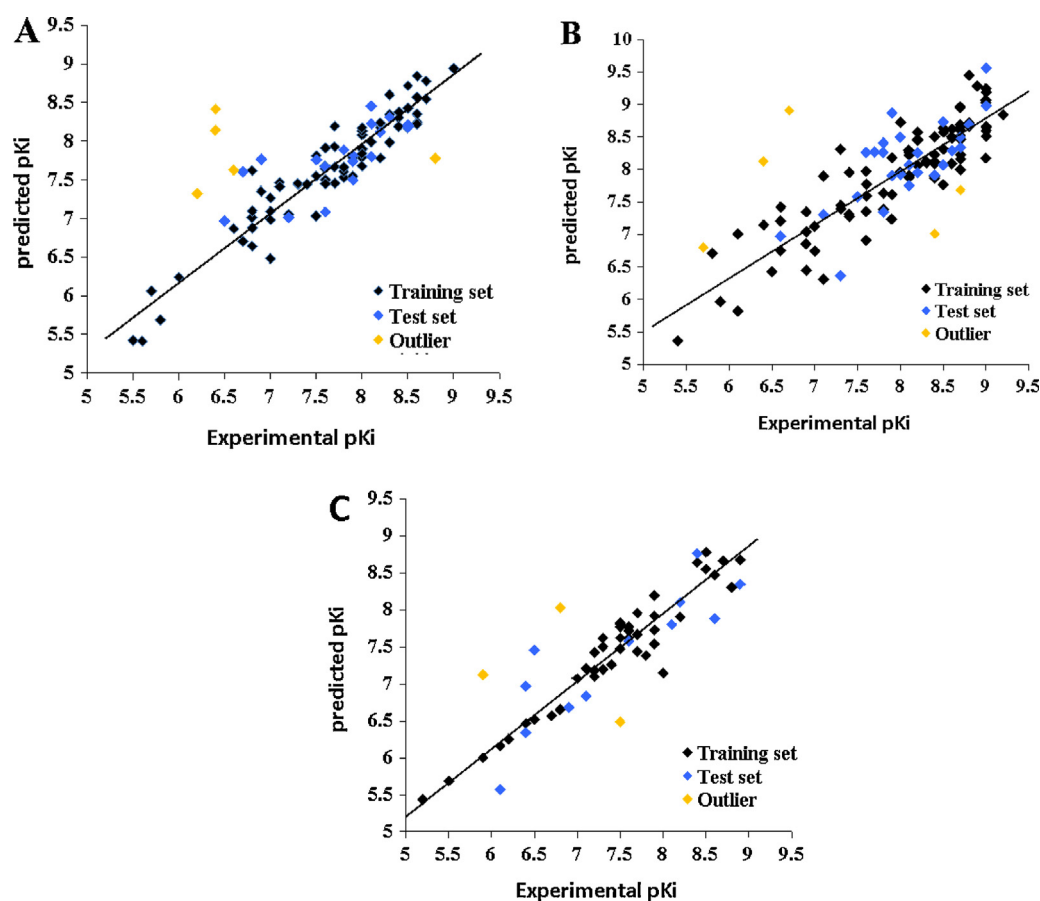


**Fig. 4.** Plot of the predicted  $pK_i$  versus the experimental  $pK_i$  values for the models based on the training (filled black rhombuses) and test (filled red rhombuses) sets. (A) I: ligand-based CoMSIA model, (B) II: ligand-based CoMSIA model, (C) III: receptor-based CoMSIA model. The solid line is the regression line for the fitted and predicted bioactivities of training compounds. The outliers in test set are shown in yellow rhombuses. (For interpretation of the references to color in this figure legend, the reader is referred to the web version of this article.)

between the experimental and predicted  $pK_i$  values are more than one logarithmic unit. Structural uniqueness underscores the outlier status of compounds. For instance, the outlier status (III: 27 and 42) are attributed to the bulky substituent (benzo-thiophenyl and  $\text{NH}(\text{CH}_2)_2\text{OH}$  group) at the pyrimidine ring, which might lead to steric bump with the active center residues. In conclusion, the high statistical values of three models add the confidence in their utility for predicting the binding affinity of the pyrimidine derivatives. And it also further corroborates the validity of pooled experimental data in the present case.

### 3.4. 3D-QSAR contour maps

In the work, 3D coefficient contour plots from the PLS models I, II and III were developed to facilitate the spatial location of the main interactions influencing the inhibitory potency. The following color codes are used to point out the interactions in S, E, H, D and A fields: green/blue/orange/cyan/magenta to indicate

favorable contour zones, yellow/red/white/purple/red-orange to represent unfavorable zones to affinity, respectively.

For the model I (Fig. 5), in agreement with experimentally determined ligand potencies at the  $A_{2A}$  AR, bulky groups are predicted to be favorable at C4 and C6 of pyrimidine ring (green region), indicating that an increase in ligand bulk would improve binding affinity. The unfavorable regions for bulky group (yellow region) are observed near the substituents at C2, C5 and C6, and also suggest the boundaries of the binding pocket of thieno[3,2-d]pyrimidine. A bulky group at C2 would have an unfavorable steric interaction with the backbone of Met270 and the side chain of Asn253. In addition, the electrostatic contour plot delineates red regions surrounding the thieno[3,2-d]pyrimidine, in which increases in partial negative ligand charges enhance the binding affinity. The orange region, which is derived in the upper part of the group at C4, is favorable for hydrophobic interaction with Ala63, Ile66 and Ile274. In contrast, white regions, the favorable position of hydrophilic interaction, emphasize the importance of the hydrophilic group at C2 and C4 for tight binding. Moreover, the group at C4 is also near a purple region,

**Table 2**  
Symbols for the molecular descriptors involved in the optimal models found.

Descriptor	Type	Description
Mor21m	3D-MoRSE	3D-MoRSE – signal 21/weighted by atomic masses
Mor22e	3D-MoRSE	3D-MoRSE – signal 22/weighted by atomic Sanderson electronegativities
Mor25m	3D-MoRSE	3D-MoRSE – signal 25/weighted by atomic masses
AlogP	Molecular properties	Ghose–Crippen octanol–water partition coefficient ( $\log P$ )
Mats5v	2D autocorrelations	Moran autocorrelation – lag 5/weighted by atomic van der Waals volumes

**Table 3**  
Statistical results of QSAR models.

Parameters	Ligand-based CoMSIA		Receptor-based CoMSIA
	I	II	III
$q^2$ <sup>a</sup>	0.53	0.48	0.60
$r_{ncv}^2$ <sup>b</sup>	0.90	0.78	0.92
SEE <sup>c</sup>	0.26	0.46	0.26
$F^d$	84.22	49.24	70.41
$r^2$ <sub>pred</sub> <sup>e</sup>	0.55	0.56	0.76
SEP <sup>f</sup>	0.58	0.70	0.56
$N_c$ <sup>g</sup>	7	6	6
$r_m^2$	0.70	0.60	0.76
Reverse $r_m^2$	0.49	0.46	0.66
Average $r_m^2$	0.59	0.53	0.71
$\Delta r_m^2$	0.21	0.14	0.10
Field contribution			
S	0.124	0.107	0.067
E	0.309	0.075	0.199
H	0.353	–	0.266
D	0.213	0.278	0.239
A	–	0.351	–
Mor21m	–	0.035	–
Mor22e	–	0.067	–
ALOGP	–	0.086	–
mor25m	–	–	0.091
mats5v	–	–	0.138

<sup>a</sup> Cross-validated correlation coefficient using the LOO methods.<sup>b</sup> Non-cross-validated correlation coefficient.<sup>c</sup> Standard error of estimate.<sup>d</sup> Ratio of  $r_{ncv}^2$  explained to unexplained =  $R^2_{ncv}/(1 - r_{ncv}^2)$ .<sup>e</sup> Predicted correlation coefficient for the test set compounds.<sup>f</sup> Standard error of prediction.<sup>g</sup> Optimal number of principal components.

which proposed that H-bond acceptors at C4 close to the side chain NH groups of Asn253 and His278 could increase the binding activity. H-bond donating group is predicted to be favorable in proximity to the substituent of the 2-furyl group at C6 (cyan region), and would functionally deliver good binding potency. In conclusion, the structural requirements of the monocyclic pyrimidine derivatives for good binding affinity are summarized in Fig. 8A as follows: (1) at C6, a limitedly bulky, electronegative and hydrophobic group is

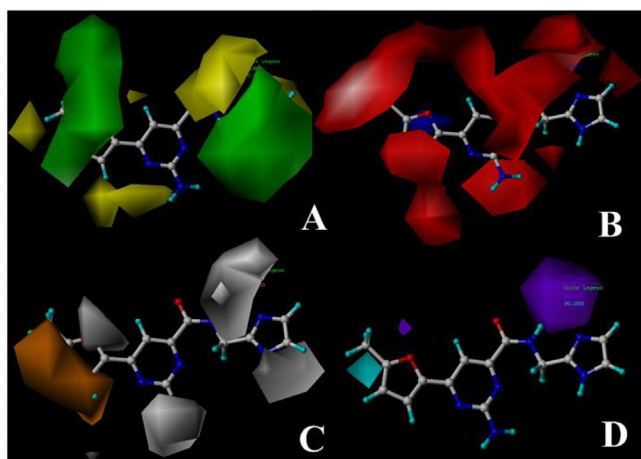


**Fig. 5.** Stdev\*coeff (A) steric, (B) electrostatic, (C) hydrophobic, (D) H-bond donor contour maps of ligand-based optimal CoMSIA model. The color code is as follows: (A) green and yellow contours indicate favorable and unfavorable bulky groups, respectively; (B) blue and red contours indicate favorable and unfavorable electropositive groups, respectively; (C) orange and white contours indicate favorable and unfavorable hydrophobic groups, respectively; (D) cyan and purple contours indicate favorable and unfavorable H-bond donor groups, respectively. The compound 92 in ball and stick is displayed as a reference. (Red atom: oxygen; blue: nitrogen). (For interpretation of the references to color in this figure legend, the reader is referred to the web version of this article.)

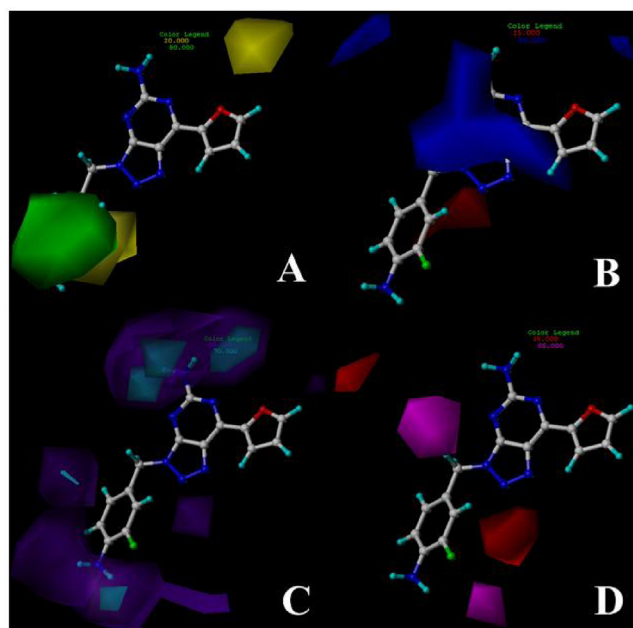


**Fig. 6.** Stdev\*coeff (A) steric, (B) electrostatic, (C) H-bond donor and (D) H-bond acceptor contour maps of ligand-based optimal CoMSIA model. The color code is as follows: (A) green and yellow contours indicate favorable and unfavorable bulky groups, respectively; (B) blue and red contours indicate favorable and unfavorable electropositive groups, respectively; (C) cyan and purple contours indicate favorable and unfavorable H-bond donor groups, respectively; (D) magenta and red-orange contours indicate favorable and unfavorable H-bond acceptor groups. The compound 111 in ball and stick is displayed as a reference. (Green atom: fluorine; red: oxygen; blue: nitrogen). (For interpretation of the references to color in this figure legend, the reader is referred to the web version of this article.)

benefic to the inhibitory binding. In most cases, substitution of 2-furyl moiety at C6 is favored for high  $A_{2A}$  AR affinity and selectivity (Azam et al., 2009). Moreover, simply adding a methyl group to this furan ring can halts the furan metabolism causing the toxicities, and restores the potency of the antagonists (Moorjani et al., 2008). (2) At C2, a small, electronegative and hydrophilic substituent would be favorable for the binding activity. (3) To display an appreciable activity, a limitedly bulky group at C4 should bear both electronegativity and hydrophilic interactions but not the role of H-bond donor. (4) The non-H groups at C5 such as methyl would affect the inhibitory activity in an unfavorable way.

In the maps of the model II (Fig. 6), the green contour at N7 of purine ring shows the interest of a substituent of an appropriate length on this moiety, while the yellow contour there indicates that (R)-substituent would lead to steric forbiddance. Similarly, other unfavorable region at the upper of the group at C6 also indicates the steric bump of bulky group with Asn253. The close inspection of the electrostatic contour allows a straightforward interpretation of the influence of substituent electronic properties on activity. It properly describes the high binding affinity of triazolo[4,5-d]pyrimidine derivatives in comparison to pyrazolo[3,4-d]pyrimidine, pyrrolo[2,3-d]pyrimidine and purine analogs. In the H-bond donor and acceptor fields, cyan contours furnish a sound for the preference of the donating group at C2 of pyrimidine ring and para-position of benzene ring, and is in close agreement with the docking result. However, the purple and magenta contours there offer readily interpretation that H-bond acceptor contributes positively to the biological activity, which also is consistent with the H-bond interactions between the group and Ala59, Phe62, Ile80 and Ala63. Acceptor groups include any functional group possessing sufficient electron density to participate in a hydrogen bond which is an important factor for the activities of the  $A_{2A}$  antagonists (Lu et al., 2011). Based on the above discussion,

the structural effects of the bicyclic derivatives on binding affinity are depicted in Fig. 8B as follows: (1) at C6 of the pyrimidine ring, a minor and electronegative group should play a role of H-bond acceptor to obtain an appreciable activity. Interestingly, the furan moiety in this series of compounds is known to be very important for high affinity binding, since its replacement with other nonfuran-containing heterocycles has showed reduced affinity for the A<sub>2A</sub> receptor (Cheong et al., 2011; Shah and Hodgson, 2010). (2) At C2 of the pyrimidine ring, a H-bond donating group would functionally deliver good potency. Generally, compounds substituted with an amino group in the C2 position have higher affinity for A<sub>2A</sub> AR rather than with a thiol or thiomethyl substituents (Azam et al., 2009). (3) at N3 of ring B (shown as in Fig. 8B), a limitedly bulky group as H-bond acceptor would affect the inhibitory activity in an favorable way. An aromatic ring attached to the nitrogen there is essential for both affinity and selectivity at the A<sub>2A</sub> antagonists.

In the maps of the model III (Fig. 7), the green area indicates the favorable effect of bulky group, while the yellow area suggests the boundaries of the pocket hosting thieno[3,2-d]pyrimidine and can be superposed perfectly onto side chains of Glu169, Met177 and Met270. Adding a methyl in position-5 of thiazolyl group would lead to steric bump with the side chains of Met177 to cause a loss of activity. Additionally, the electrostatic contour offers readily interpretable electronegative signal by red polyhedral, indicating that the electronegative substituent at the pyrimidine ring is benefic for the binding affinity. The white contours are mapped well with the hydrophilic surface of the active site including Glu169, Asn181, Asn253 and Cys254 which likely interact with the groups at C2 and C6. Moreover, the H-bond maps suggest the H-bond accepting group at C2 and donating group at C6 of the pyrimidine ring are preferable for the binding by interacting with the side chain imidazole group of His250 and the amino groups of Asn253 and Glu169. Thus, the structural requirements of the thieno[3,2-d]pyrimidines derivatives for good binding affinity are depicted in Fig. 8C as follows: (1) at C6 of the pyrimidine ring, an electronegative, hydrophilic and limitedly bulky group as H-bond donor is favorable for the increase of the inhibitory activity. (2) At C2 of the pyrimidine ring, a small and electronegative group as H-bond donor is well tolerated and would functionally deliver good potency. A<sub>2A</sub> AR affinity and selectivity over A<sub>1</sub> AR is particularly noteworthy when the C-2 substituent is a small lipophilic group such as alkyl or dialkylamino (Azam et al., 2009).

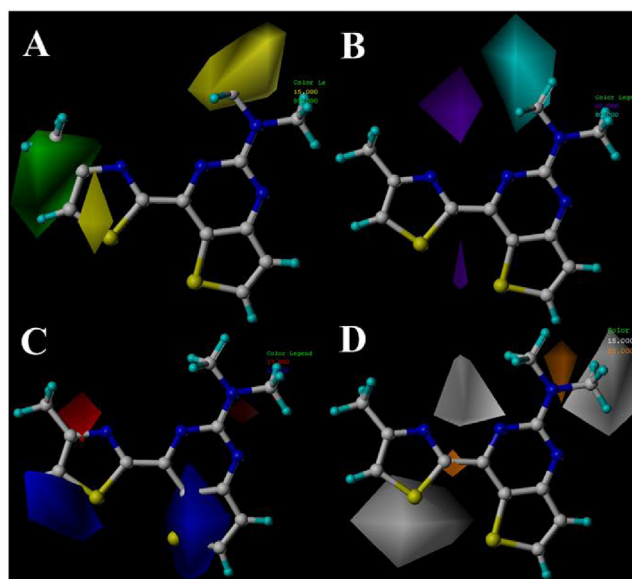


**Fig. 7.** Stdev\*coeff (A) steric, (B) H-bond donor, (C) electrostatic, (D) hydrophobic contour maps of receptor-based optimal CoMSIA model. The color code is as follows: (A) green and yellow contours indicate favorable and unfavorable bulky groups, respectively; (B) cyan and purple contours indicate favorable and unfavorable H-bond donor groups, respectively; (C) blue and red contours indicate favorable and unfavorable electropositive groups, respectively; (D) orange and white contours indicate favorable and unfavorable hydrophobic groups, respectively. The compound 45 in ball and stick is displayed as a reference. (yellow atom: sulfur; blue: nitrogen). (For interpretation of the references to color in this figure legend, the reader is referred to the web version of this article.)

Overall, to all the monocyclic and bicyclic pyrimidine derivatives, changes in the inhibitory activity could be rationalized by modifying the compounds based on the key structural features: (i) a minor/large group with negative charge at C2/C6 of the pyrimidine ring respectively contribute favorably to the biological activity of the antagonist. Interestingly, a group like N–H at C2 is required to provide a H-bond donor for a good interaction with all the adenosine receptors (Azam et al., 2009). (ii) Especially for the bicyclic derivatives, the bicyclic contain the higher electron density of the ring, then the more potent for the antagonists.

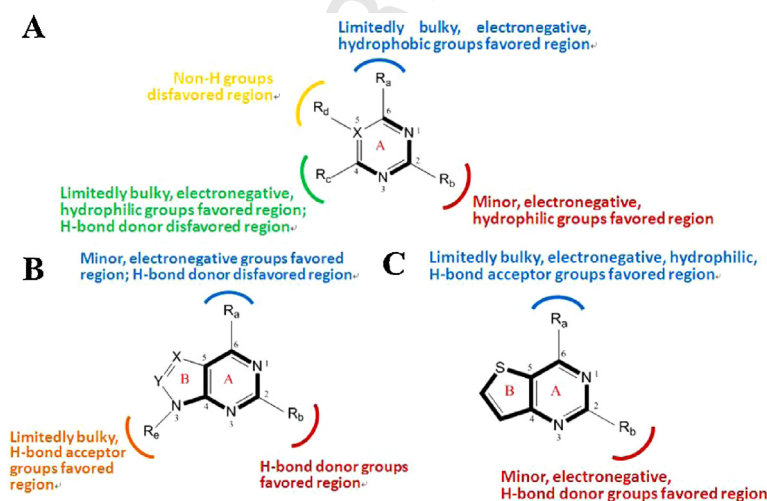


**Fig. 8.** Structural features obtained from optimal CoMSIA model. (A): I model (X=C/N); (B): II model (X=C/N, Y=C/N); (C): III model. The common substructure is shown in bold.

#### 4. Conclusion

There is now accumulating evidence that A<sub>2A</sub> AR antagonists may provide a novel therapy for the treatment of Parkinson's disease with lower risk of dyskinesias. The present study confirms and reinforces the validity of the interaction mode of A<sub>2A</sub> AR with monocyclic and bicyclic pyrimidine derivatives, and provides insights into the structural requirements of the derivatives for high A<sub>2A</sub> AR affinity. The pyrimidine derivatives are positioned toward TM2, 3, 5, 6 and 7 of A<sub>2A</sub> AR, anchored by the aromatic stacking with Phe168(5.29), hydrogen bonding interactions with Glu169(5.30) and Asn253(6.55), as well as non-polar interactions with the receptor. Additionally, the derivatives have an aromatic group extending deeper into the binding pocket and/or flexible extensions toward the extracellular opening of the pocket. The comparison of the binding poses for the above antagonists with ZM241385, XAC and caffeine in the crystal structure reveals similarities in the side chains of amino acid residues involved in ligand recognition. Moreover, the calculated binding free energies with the biggest contribution of van der Waals confirm the reasonableness of the binding modes. On the other hand, the ligand/receptor-based 3D-QSAR studies on the derivatives were performed using CoMFA and CoMSIA tools with the addition of molecular descriptors. The models display high statistical quality and the good consistency between the maps and the docking results, which add the confidence in their utility for predicting the binding affinity of the antagonists. Moreover, the  $r_m^2$  metrics suggest the predictability of the models. The resulting contour maps correlate well with the structural features of the pyrimidine derivatives as the above discussions, which might be helpful in future rational design of novel candidate for the potential treatment of Parkinson's disease.

#### Acknowledgements

This work is financially supported by State Key Laboratory of the Discovery and Development of Novel Pesticide (No. 201101). This research is also supported by high-performance computing platform of Northwest A & F University.

#### Appendix A. Supplementary data

Supplementary data associated with this article can be found, in the online version, at <http://dx.doi.org/10.1016/j.biosystems.2013.04.003>.

#### References

- Azam, F., Ibn-Rajab, I.A., Alruaid, A.A., 2009. Adenosine A2A receptor antagonists as novel anti-Parkinsonian agents: a review of structure–activity relationships. *Pharmazie* 64 (12), 771–795.
- Ballesteros, J.A., Weinstein, H., 1995. [19] Integrated methods for the construction of three-dimensional models and computational probing of structure–function relations in G protein-coupled receptors. In: Stuart, C. (Ed.), *Methods in Neurosciences*, vol. 25. Academic Press, pp. 366–428.
- Bara-Jimenez, W., Sherzai, A., Dimitrova, T., Favit, A., Bibbiani, F., Gillespie, M., Morris, M.J., Mouradian, M.M., Chase, T.N., 2003. Adenosine A(2A) receptor antagonist treatment of Parkinson's disease. *Neurology* 61 (3), 293–296.
- Berendsen, H.J., Grigera, J.R., Stratsma, T.P., 1987. The missing term in effective pair potentials. *The Journal of Physical Chemistry* 91, 6269–6271.
- Blackburn, M.R., Vance, C.O., Morschl, E., Wilson, C.N., 2009. Adenosine receptors and inflammation. *Handbook of Experimental Pharmacology* 193, 215–269.
- Bussi, G., Donadio, D., Parrinello, M., 2007. Canonical sampling through velocity rescaling. *The Journal of Physical Chemistry* 126 (1), 014101.
- Carlsson, J., Yoo, L., Gao, Z.G., Irwin, J.J., Shoichet, B.K., Jacobson, K.A., 2010. Structure-based discovery of A2A adenosine receptor ligands. *Journal of Medicinal Chemistry* 53 (9), 3748–3755.
- Case, D.A.D., Cheatham, T.A., Simmerling, T.E., Wang, C.L., Duke, J., Luo, R.E., Crowley, R., Walker, M., Zhang, R.C., Merz, W., Wang, K.M., Hayik, B., Roitberg, S., Seabra, A., Kolossvary, G., Wong, I., Paesani, K.F., Vanicek, F., Wu, J., Brozell, X., Steinbrecher, S.R., Gohlke, T., Yang, H., Tan, L., Mongan, C., Hornak, J., Cui, V., Mathews, G.,

- Seetin, D.H., Sagui, M.G., Babin, C., Kollman, V.P.A., 2008. AMBER 10. University of California, San Francisco.
- Cheong, S.L., Venkatesan, G., Paira, P., Jothibasu, R., Mandel, A.L., Federico, S., Spalluto, G., Pastorin, G., 2011. Pyrazolo derivatives as potent adenosine receptor antagonists: an overview on the structure–activity relationships. *International Journal of Medicinal Chemistry*, <http://dx.doi.org/10.1155/2011/480652>.
- Clark, M., Cramer, R.D., Van Opdenbosch, N., 1989. Validation of the general purpose tripos 5.2 force field. *Journal of Computational Chemistry* 10 (8), 982–1012.
- Congreve, M., Andrews, S.P., Dore, A.S., Hollenstein, K., Hurrell, E., Langmead, C.J., Mason, J.S., Ng, I.W., Tehan, B., Zhukov, A., Weir, M., Marshall, F.H., 2012. Discovery of 1,2,4-triazine derivatives as adenosine A(2A) antagonists using structure based drug design. *Journal of Medicinal Chemistry* 55 (5), 1898–1903.
- Cristalli, G., Lambertucci, C., Marucci, G., Volpini, R., Dal Ben, D., 2008. A2A adenosine receptor and its modulators: overview on a druggable GPCR and on structure–activity relationship analysis and binding requirements of agonists and antagonists. *Current Pharmaceutical Design* 14 (15), 1525–1552.
- Culler, D.E., Karp, R.M., Patterson, D., Sahay, A., Santos, E.E., Schausser, K.E., Subramanian, R., Eicken, T., 1996. LogP: a practical model of parallel computation. *Communications of the ACM* 39 (11), 78–85.
- Darden, T., York, D., Pedersen, L., 1993. Particle mesh Ewald – an  $N \log(N)$  method for Ewald sums in large systems. *Journal of Chemical Physics* 98 (12), 10089–10092.
- Dore, A.S., Robertson, N., Errey, J.C., Ng, I., Hollenstein, K., Tehan, B., Hurrell, E., Bennett, K., Congreve, M., Magnani, F., Tate, C.G., Weir, M., Marshall, F.H., 2011. Structure of the adenosine A(2A) receptor in complex with ZM241385 and the xanthines XAC and caffeine. *Structure* 19 (9), 1283–1293.
- Drabczynska, A., Zygmunt, M., Sapa, J., Filippek, B., Muller, C.E., Kiec-Kononowicz, K., 2011. Antiparkinsonian effects of novel adenosine A(2A) receptor antagonists. *Archiv der Pharmazie* 344 (1), 20–27.
- Fenu, S., Pinna, A., Ongini, E., Morelli, M., 1997. Adenosine A2A receptor antagonism potentiates L-DOPA-induced turning behaviour and c-fos expression in 6-hydroxydopamine-lesioned rats. *European Journal of Pharmacology* 321 (2), 143–147.
- Fishman, P., Bar-Yehuda, S., Synowitz, M., Powell, J.D., Klotz, K.N., Gessi, S., Borea, P.A., 2009. Adenosine receptors and cancer. *Handbook of Experimental Pharmacology* 193, 399–441.
- Frau, L., Borsini, F., Wardas, J., Khairnar, A.S., Schintu, N., Morelli, M., 2011. Neuroprotective and anti-inflammatory effects of the adenosine A(2A) receptor antagonist ST1535 in a MPTP mouse model of Parkinson's disease. *Synapse* 65 (3), 181–188.
- Gasteiger, J., Marsili, M., 1980. Iterative partial equalization of orbital electronegativity—a rapid access to atomic charges. *Tetrahedron* 36 (22), 3219–3228.
- Gillespie, R.J., Adams, D.R., Bebbington, D., Benwell, K., Cliffe, I.A., Dawson, C.E., Dourish, C.T., Fletcher, A., Gaur, S., Giles, P.R., Jordan, A.M., Knight, A.R., Knutsen, L.J., Lawrence, A., Lerpiniere, J., Misra, A., Porter, R.H., Pratt, R.M., Shepherd, R., Upton, R., Ward, S.E., Weiss, S.M., Williamson, D.S., 2008a. Antagonists of the human adenosine A2A receptor. Part 1. Discovery and synthesis of thieno[3,2-d]pyrimidine-4-methanone derivatives. *Bioorganic & Medicinal Chemistry Letters* 18 (9), 2916–2919.
- Gillespie, R.J., Cliffe, I.A., Dawson, C.E., Dourish, C.T., Gaur, S., Giles, P.R., Jordan, A.M., Knight, A.R., Lawrence, A., Lerpiniere, J., Misra, A., Pratt, R.M., Todd, R.S., Upton, R., Weiss, S.M., Williamson, D.S., 2008b. Antagonists of the human adenosine A2A receptor. Part 2. Design and synthesis of 4-arylthieno[3,2-d]pyrimidine derivatives. *Bioorganic & Medicinal Chemistry Letters* 18 (9), 2920–2923.
- Gillespie, R.J., Cliffe, I.A., Dawson, C.E., Dourish, C.T., Gaur, S., Jordan, A.M., Knight, A.R., Lerpiniere, J., Misra, A., Pratt, R.M., Roffey, J., Stratton, G.C., Upton, R., Weiss, S.M., Williamson, D.S., 2008c. Antagonists of the human adenosine A2A receptor. Part 3: Design and synthesis of pyrazolo[3,4-d]pyrimidines, pyrrolo[2,3-d]pyrimidines and 6-arylpurines. *Bioorganic & Medicinal Chemistry Letters* 18 (9), 2924–2929.
- Gillespie, R.J., Bamford, S.J., Botting, R., Comer, M., Denny, S., Gaur, S., Griffin, M., Jordan, A.M., Knight, A.R., Lerpiniere, J., Leonardi, S., Lightowler, S., McAteer, S., Merrett, A., Misra, A., Padfield, A., Reece, M., Saadi, M., Selwood, D.L., Stratton, G.C., Surry, D., Todd, R., Tong, X., Ruston, V., Upton, R., Weiss, S.M., 2009a. Antagonists of the human A(2A) adenosine receptor. 4. Design, synthesis, and preclinical evaluation of 7-aryltriazolo[4,5-d]pyrimidines. *Journal of Medicinal Chemistry* 52 (1), 33–47.
- Gillespie, R.J., Bamford, S.J., Clay, A., Gaur, S., Haymes, T., Jackson, P.S., Jordan, A.M., Klenke, B., Leonardi, S., Liu, J., Mansell, H.L., Ng, S., Saadi, M., Simmonite, H., Stratton, G.C., Todd, R.S., Williamson, D.S., Yule, I.A., 2009b. Antagonists of the human A(2A) receptor. Part 6: Further optimization of pyrimidine-4-carboxamides. *Bioorganic & Medicinal Chemistry* 17 (18), 6590–6605.
- Gillespie, R.J., Bamford, S.J., Gaur, S., Jordan, A.M., Lerpiniere, J., Mansell, H.L., Stratton, G.C., 2009c. Antagonists of the human A(2A) receptor. Part 5: Highly bio-available pyrimidine-4-carboxamides. *Bioorganic & Medicinal Chemistry Letters* 19 (10), 2664–2667.
- Gillespie, R.J., Bamford, S.J., Botting, R., Comer, M., Denny, S., Gaur, S., Griffin, M., Jordan, A.M., Knight, A.R., Lerpiniere, J., Leonardi, S., Lightowler, S., McAteer, S., Merrett, A., Misra, A., Padfield, A., Reece, M., Saadi, M., Selwood, D.L., Stratton, G.C., Surry, D., Todd, R., Tong, X., Ruston, V., Upton, R., Weiss, S.M., 2009d. Antagonists of the Human A(2A) Adenosine Receptor. 4. Design, synthesis, and preclinical evaluation of 7-aryltriazolo[4,5-d]pyrimidines. *Journal of Medicinal Chemistry* 52 (1), 33–47.
- Headrick, J.P., Lasley, R.D., 2009. Adenosine receptors and reperfusion injury of the heart. *Handbook of Experimental Pharmacology* 193, 189–214.

- Hess, B., Kutzner, C., van der Spoel, D., Lindahl, E., 2008. GROMACS 4: algorithms for highly efficient, load-balanced, and scalable molecular simulation. *Journal of Chemical Theory and Computation* 4 (3), 435–447.
- Hummer, G., Rasaiah, J.C., Noworyta, J.P., 2001. Water conduction through the hydrophobic channel of a carbon nanotube. *Nature* 414 (6860), 188–190.
- Ivanov, A.A., Palyulin, V.A., Zefirov, N.S., 2007. Computer aided comparative analysis of the binding modes of the adenosine receptor agonists for all known subtypes of adenosine receptors. *Journal of Molecular Graphics and Modelling* 25 (5), 740–754.
- Ivanov, A.A., Barak, D., Jacobson, K.A., 2009. Evaluation of homology modeling of G-protein-coupled receptors in light of the A(2A) adenosine receptor crystallographic structure. *Journal of Medicinal Chemistry* 52 (10), 3284–3292.
- Jaakola, V.P., Griffith, M.T., Hanson, M.A., Cherezov, V., Chien, E.Y., Lane, J.R., Ijzerman, A.P., Stevens, R.C., 2008. The 2.6 angstrom crystal structure of a human A2A adenosine receptor bound to an antagonist. *Science* 322 (5905), 1211–1217.
- Jaakola, V.P., Lane, J.R., Lin, J.Y., Katritch, V., Ijzerman, A.P., Stevens, R.C., 2010. Identification and characterization of amino acid residues essential for human A2A adenosine receptor: ZM241385 binding and subtype selectivity. *The Journal of Biological Chemistry*. <http://dx.doi.org/10.1074/jbc.M109.096974>.
- Jenner, P., Mori, A., Hauser, R., Morelli, M., Fredholm, B.B., Chen, J.F., 2009. Adenosine, adenosine A2A antagonists, and Parkinson's disease. *Parkinsonism & Related Disorders* 15 (6), 406–413.
- Kanda, T., Jackson, M.J., Smith, L.A., Pearce, R.K., Nakamura, J., Kase, H., Kuwana, Y., Jenner, P., 1998. Adenosine A2A antagonist: a novel antiparkinsonian agent that does not provoke dyskinesia in parkinsonian monkeys. *Annals of Neurology* 43 (4), 507–513.
- Kase, H., Aoyama, S., Ichimura, M., Ikeda, K., Ishii, A., Kanda, T., Koga, K., Koike, N., Kurokawa, M., Kuwana, Y., Mori, A., Nakamura, J., Nonaka, H., Ochi, M., Saki, M., Shimada, J., Shindou, T., Shiozaki, S., Suzuki, F., Takeda, M., Yanagawa, K., Richardson, P.J., Jenner, P., Bedard, P., Borrelli, E., Hauser, R.A., Chase, T.N., 2003. Progress in pursuit of therapeutic A2A antagonists: the adenosine A2A receptor selective antagonist KW6002: research and development toward a novel nondopaminergic therapy for Parkinson's disease. *Neurology* 61 (11 (Suppl. 6)), S97–S100.
- Kim, J., Wess, J., van Rhee, A.M., Schoneberg, T., Jacobson, K.A., 1995. Site-directed mutagenesis identifies residues involved in ligand recognition in the human A2a adenosine receptor. *Journal of Biological Chemistry* 270 (23), 13987–13997.
- Kim, S.K., Gao, Z.G., Van Rompaey, P., Gross, A.S., Chen, A., Van Calenbergh, S., Jacobson, K.A., 2003. Modeling the adenosine receptors: comparison of the binding domains of A2A agonists and antagonists. *Journal of Medicinal Chemistry* 46 (23), 4847–4859.
- Kiran, K.M., Annapurna, R.C., Prameela, S.N.J., Uma, V., 2012. Pharmacophore mapping and in silico screening to identify new potent leads for A2A adenosine receptor, as antagonists. *Journal of Receptors and Signal Transduction* 32 (2), 102–113.
- Knutsen, L.J., Weiss, S.M., 2001. KW-6002 (Kyowa Hakko Kogyo). *Current Opinion in Investigational Drugs* 2 (5), 668–673.
- Langmead, C.J., Andrews, S.P., Congreve, M., Errey, J.C., Hurrell, E., Marshall, F.H., Mason, J.S., Richardson, C.M., Robertson, N., Zhukov, A., Weir, M., 2012. Identification of novel adenosine A(2A) receptor antagonists by virtual screening. *Journal of Medicinal Chemistry* 55 (5), 1904–1909.
- Lu, P., Wei, X., Zhang, R., Yuan, Y., Gong, Z., 2011. Prediction of the binding affinities of adenosine A<sub>2A</sub> receptor antagonists based on the heuristic method and support vector machine. *Medicinal Chemistry Research* 20 (8), 1220–1228.
- Michielan, L., Bacilieri, M., Schiesaro, A., Bolcato, C., Pastorin, G., Cacciari, B., Klotz, K.N., Kaseda, C., Moro, S., 2008. Linear and nonlinear 3D-QSAR approaches in tandem with ligand-based homology modeling as a computational strategy to depict the pyrazolo-triazolo-pyrimidine antagonists binding site of the human adenosine A2A receptor. *Journal of Chemical Information and Modeling* 48 (2), 350–363.
- Moorjani, M., Zhang, X., Chen, Y., Lin, E., Rueter, J.K., Gross, R.S., Lanier, M.C., Tellew, J.E., Williams, J.P., Lechner, S.M., Malany, S., Santos, M., Ekhlassi, P., Castro-Palomino, J.C., Crespo, M.I., Prat, M., Gual, S., Diaz, J.L., Saunders, J., Slee, D.H., 2008. 2,6-Diaryl-4-phenacylamino-pyrimidines as potent and selective adenosine A(2A) antagonists with reduced hERG liability. *Bioorganic & Medicinal Chemistry Letters* 18 (4), 1269–1273.
- Morelli, M., Carta, A.R., Jenner, P., 2009. Adenosine A2A receptors and Parkinson's disease. *Handbook of Experimental Pharmacology* 193, 589–615.
- Morris, G.M., Goodsell, D.S., Huey, R., Olson, A.J., 1996. Distributed automated docking of flexible ligands to proteins: parallel applications of AutoDock 2.4. *Journal of Computer-Aided Molecular Design* 10 (4), 293–304.
- Morris, G.M., Goodsell, D.S., Halliday, R.S., Huey, R., Hart, W.E., Belew, R.K., Olson, A.J., 1998. Automated docking using a Lamarckian genetic algorithm and an empirical binding free energy function. *Journal of Computational Chemistry* 19 (14), 1639–1662.
- Ojha, P.K., Mitra, I., Das, R.N., Roy, K., 2011. Further exploring rm2 metrics for validation of QSPR models. *Chemometrics and Intelligent Laboratory Systems* 107, 194–205.
- Ongini, E., Adami, M., Ferri, C., Bertorelli, R., 1997. Adenosine A2A receptors and neuroprotection. *Annals of the New York Academy of Sciences* 825, 30–48.
- Osterberg, F., Morris, G.M., Sanner, M.F., Olson, A.J., Goodsell, D.S., 2002. Automated docking to multiple target structures: incorporation of protein mobility and structural water heterogeneity in AutoDock. *Proteins* 46 (1), 34–40.
- Parrinello, M.R., 1981. A polymorphic transitions in single crystals: a new molecular dynamics method. *Journal of Applied Physics* 52 (12), 7182–7190.
- Richardson, P.J., Kase, H., Jenner, P.G., 1997. Adenosine A(2A) receptor antagonists as new agents for the treatment of Parkinson's disease. *Trends in Pharmacological Sciences* 18 (9), 338–344.
- Roy, K., Chakraborty, P., Mitra, I., Ojha, P.K., Kar, S., Das, R.N., 2013. Some case studies on application of  $r_m^2$  metrics for judging quality of QSAR predictions: emphasis on scaling of response data. *Journal of Computational Chemistry* 34, 1071–1082, <http://dx.doi.org/10.1002/jcc.23231>.
- Roy, K., Mitra, I., 2012. On the use of the metric  $r_m^2$  as an effective tool for validation of QSAR models in computational drug design and predictive toxicology. *Mini-Reviews in Medicinal Chemistry* 12, 491–504.
- Roy, K., Mitra, I., Kar, S., Ojha, P.K., Das, R.N., Kabir, H., 2012. Comparative studies on some metrics for external validation of QSPR models. *Journal of Chemical Information and Modeling* 52, 396–408.
- Sanner, M.F., Olson, A.J., Spehner, J.C., 1996. Reduced surface: an efficient way to compute molecular surfaces. *Biopolymers* 38 (3), 305–320.
- Sali, A., Blundell, T.L., 1993. Comparative protein modelling by satisfaction of spatial restraints. *Journal of Molecular Biology* 234 (3), 779–815.
- Sauer, R., Maurinsh, J., Reith, U., Fulle, F., Klotz, K.N., Muller, C.E., 2000. Water-soluble phosphate prodrugs of 1-propargyl-8-styrylxanthine derivatives, A(2A)-selective adenosine receptor antagonists. *Journal of Medicinal Chemistry* 43 (3), 440–448.
- Schwarzschild, M.A., Agnati, L., Fuxe, K., Chen, J.F., Morelli, M., 2006. Targeting adenosine A2A receptors in Parkinson's disease. *Trends in Neurosciences* 29 (11), 647–654.
- Shah, U., Hodgson, R., 2010. Recent progress in the discovery of adenosine A(2A) receptor antagonists for the treatment of Parkinson's disease. *Current Opinion in Drug Discovery & Development* 13 (4), 466–480.
- Wang, J., Wolf, R.M., Caldwell, J.W., Kollman, P.A., Case, D.A., 2004. Development and testing of a general amber force field. *Journal of Computational Chemistry* 25 (9), 1157–1174.
- Wang, X., Yang, W., Xu, X., Zhang, H., Li, Y., Wang, Y., 2010. Studies of benzothiadiazine derivatives as hepatitis C virus NS5B polymerase inhibitors using 3D-QSAR, molecular docking and molecular dynamics. *Current Medicinal Chemistry* 17 (25), 2788–2803.
- Zhang, H.X., Li, Y., Wang, X., Xiao, Z.T., Wang, Y.H., 2011. Insight into the structural requirements of benzothiadiazine scaffold-based derivatives as hepatitis C virus NS5B polymerase inhibitors using 3D-QSAR, molecular docking and molecular dynamics. *Current Medicinal Chemistry* 18 (26), 4019–4028.